Fachtagung "Lasermethoden in der Strömungsmesstechnik"
9. – 11. September 2014, Karlsruhe

Numerische Validierung der experimentellen Daten eines optimierten HAWT

Numerical Validation of the Experimental Data of an Optimized HAWT

Ali Al-Abadi[1,2], Özgür Ertunç[3], Frederik Berger[1], Julie Seok[1] & Antonio Delgado[1]
[1]Institute of Fluid Mechanics, Friedrich-Alexander-University Erlangen-Nuremberg, Germany
[2]AlKhwarizmi Collage of Engineering - University of Baghdad, Baghdad, Iraq
[3]Ozyegin University, Mechanical Engineering Department, Istanbul, Turkey

Schlagworte: Numerische Simulation, Optimierung, HAWT
Key words: Numerical simulation, Optimization, HAWT

Abstract

In this work, an optimized HAWT has been analyzed numerically for validating its experimental data. The 3-D steady state CFD simulations have been performed in Star CCM+ with the RANS k-ω SST turbulence model. A single blade is modelled in a 120± fraction of a cylindrical domain, using periodic boundaries. Rotational effects are modelled by a frozen rotor approach. The design and off-design performance are investigated. The power coefficient was in good agreement with experimental data. Of special interest are the limitations of steady CFD investigations for the case of partially stalled conditions. It is shown that RANS investigations can provide good power indication despite boundary layer separation and reversal flow. Additional information that can be obtained from simulation such as radial flow, detached boundary layer and flow circulation are presented as well.

Introduction

Computational Fluid Dynamics (CFD) Simulations offer great possibilities for the aerodynamic design and validation of Horizontal Axis Wind Turbine (HAWT) blades. They are reliable to study the flow over large structures, without the need for scaling. Furthermore, they are effective and practical in providing insights to flow phenomena such as three-dimensional, unsteady prediction, stall, boundary layer, flow separation and surface flow analysis. However, the quality and effectiveness of the computations are dependent on the applied physical models, Sumner et al. 2010. CFD methods involve many turbulent models to solve different flow structures. Carcangiu et at. 2007, performed steady state Reynolds averaged Navier-Stokes (RANS) computations, with the k-ω Shear Stress Transport (SST) turbulence model to study the rotational effects on the boundary layer behaviour of wind turbine blades. Mahu et al. 2011, modelled and simulated the NREL Phase IV rotor with the same model. Anjuri 2012, applied this turbulence model with an added transition model by Langtry and Menter for simulations of the NREL Phase IV rotor, with good agreement to published data. Kirrkamm et al. 2010, applied this turbulence model but performed the simulations as Unsteady Reynolds Averaged Navier-Stokes (URANS), in order to obtain a more realistic insight into the separated flow regions on the blade. Although the number of mesh cells was chosen low, the computational effort was considered elaborate. Carcangiu 2008, additionally carried out

wake investigations with RANS simulations. Due to the turbulent character of wakes, especially in the far wake, Vermeer et al. 2003, recommend unsteady Large Eddy Simulations (LES) or Detached Eddy Simulations (DES) for investigations. Wussow et al. 2007, applied a LES to study the wake of the Enercon E66 turbine. They applied a turbulent wind field inlet and compared it to corresponding field measurements over a time period of several minutes. Their simulations matched the measurements quite well. In general, the numerical methods are robust and reliable when the flow is steady and uniform.

In the present study, a validation of an optimized turbine performance with RANS numerical simulations of STAR-CCM+ was performed. The simulations are performed as steady state RANS with the k-ω SST turbulence model. The operating power coefficient at the design and off-design tip speed ratios is investigated and compared to experimental data. The flow over the wind turbine blade at different angles of attack is assessed in regards of separation and three dimensional flow on the blade.

Numerical Settings

A blade geometry, which was optimized with the TMASO method, Al-Abadi et al. 2013, is validated with the numerical simulation. It is imported as an IGES file to Star CCM+. The computational domain was chosen to be cylindrical. The simulations of the three-bladed HAWT were performed as steady state simulations, with a geometrically constant inlet wind velocity. Therefore, it was possible to make use of the periodicity of the model. The simulation of a 120° fraction of a cylindrical domain with one blade was sufficient. Dimensions are given as multiples of the radius of the turbine (R = 0.25m), as shown in Figure 1. The axis of the cylinder fraction is the axis of rotation. The blade geometry is enclosed and subtracted from the inner domain. The connection is at the inner domain interface surfaces that have corresponding interface surfaces in the outer domain. With the periodic boundaries, a full cylinder is modelled. The outlet boundaries are chosen in the far-field so that the flow over the blade is not affected by interactions with these boundaries. The basic dimensions of the inner and the outer domain are shown in Figure 1.

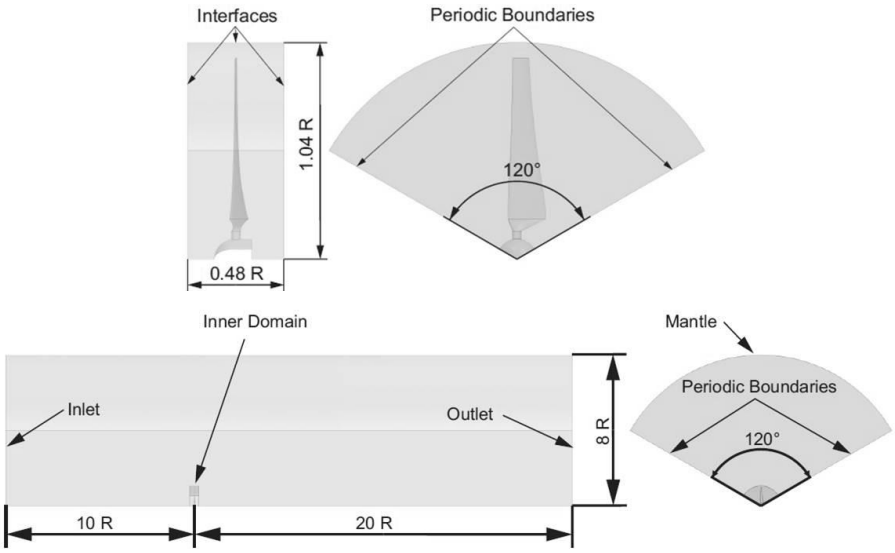

Figure 1: Geometrical configuration of inner and outer domains

Since the results of a CFD simulation depend strongly on the size and quality of the grid, the meshing process, therefore, is one of the most important steps for a simulation, Hirsch 2008.

The volume mesh consists of polyhedral elements with prisms for walls, where boundary layers form, CD-ADAPCO 2013. The surface mesh size is set by the base size of the domain. For surfaces of interest this value is adjusted. The polyhedral volume mesh size is defined by the base size. Adjustments are made by volumetric controls that are presented by external CAD volumes for the near and far wake. These are used for controlling the refinement of the entire computational domain. Main mesh settings were defined globally for all domains. The surface growth rate is set to 1.3 and the polyhedra expansion ratio is set to 1.05. CD-ADAPCO 2013, suggests values between 1.05 – 1.15 for incompressible external aerodynamic simulations, for a slow volume growth of the polyhedra. The prism layer settings, which are dependent on the used turbulence model and the origin of the following values, are set. 21 prism layers are applied with a total thickness of 0.0024m and a stretching ratio of 1.2. The number of cells and faces for the model are $4*10^6$ and $22.15*10^6$, respectively. The mesh distribution is shown in figure 2.

The physical configuration for the model was set to a three dimensional and steady state. The RANS k-ω SST model is applied, where it is designed for the simulation of external aeronautic flows with adverse pressure gradients and separation, Menter et al. 2003.

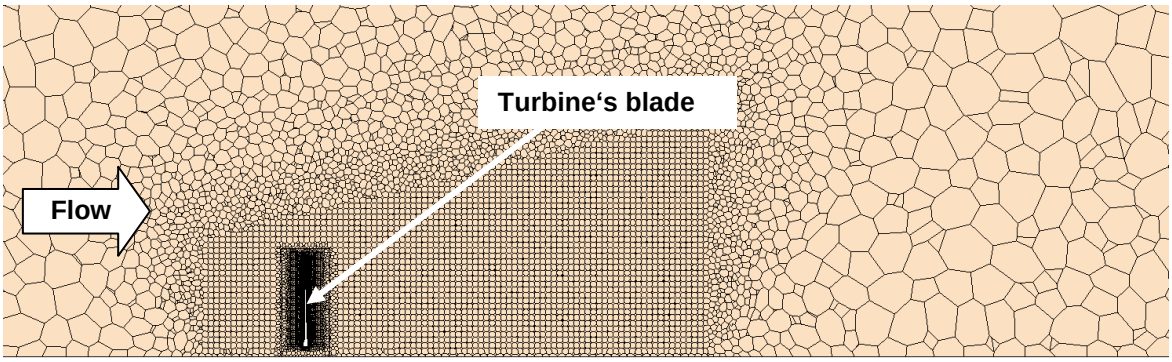

Figure 2: Polyhedral mesh distribution

The distance for the first boundary layer cell from the blade surface is estimated based on chord Reynolds number (Re,c). The first prism layer has a wall distance of less than the boundary layer thickness (y<δ). In steady state simulations, the movement or rotation of objects can be modelled by additional reference frames. Here, two reference frames are applied. The outer domain is in the stationary inertial lab reference frame. The Inner domain are in a rotational reference frame. The axis of the rotational reference frame is the axis of rotation.

Finally, with the implementation of boundary condition values, the system can be solved numerically. The values of the model are stated in Table 1. The direction of the velocity inlet is normal with regard to the boundary faces. Further, the turbulence intensity is set to a low level at 0.01.

Outer Domain	
Inlet	Velocity inlet
Outlet	Pressure outlet
Mantle	Slip wall
Interfaces	In-place interface
Periodic boundaries	Periodic interface
Inner Domain	
Interfaces	In-place interface
Periodic boundaries	Periodic interface
Blade portions	No-slip wall

Table 1: Boundary conditions

Results

The power coefficient is plotted over the tip speed ratio for the simulations in comparison to the provided experimental data as shown in Figure 3. The simulated points in the design region are in good agreement with the experimental data. The design region is within the tip speed ratio range of $3.9 < \lambda < 4.7$. The design point is at $\lambda = 4.1$, which corresponds to the design blade angle of attack of $\alpha_{design} = 8°$.
A decrease in tip speed ratio causes an increase in angle of attack along the whole blade span, and vice versa. In the low angle of attack region, the simulation still in its good agreement and reflects the same experimental data trend. In the high angle of attack region, both results reveal a sharp decrease of power coefficient due to the beginning of stall. In the simulations, a more gentle decrease in power coefficient can be seen. The simulations were performed under the assumption of mainly steady flow phenomena. However, the flow in separated flow regions is highly unsteady and thus the steady RANS model may not be appropriate to investigate these states.

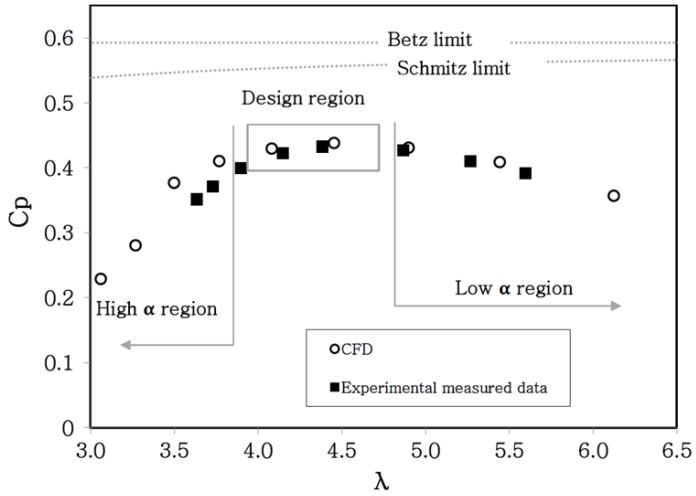

Figure 3: Power coefficient over tip speed ratio

The tangential component of the velocity, seen from the rotating blade, is shown along velocity streamlines in Figure 4 for low, design and high angle of attack.
For the low and design angle of attack configurations, the flow over the blade seems largely undisturbed at all sections. However, there is a reversed boundary layer flow at the trailing edge. As can be seen from the figure; the maximum velocity of the reversal flow increases with increasing of the angle of attack. For the first high angle of attack configuration at $\lambda = 3.5$, there is clear separation at the mid-section, whereas the root section and the tip section seem to be less affected. For the tip speed ratio of $\lambda = 3.06$, the flow on the mid span suction side is detached completely. In addition, an obvious flow separation appears in both root and tip regions. The root section shows an earlier separation, which is the separation bubble near the leading edge. Due to large separated areas, the applicability of the RANS model has to be questioned for the second high angle of attack simulation.

For a better understanding of the differences between the flow over the tested sections, the three dimensional flow on the blade surface is investigated. Figure 5 shows streamlines alongside the pressure on the suction (S) and pressure (P) side of the blade for the low angle of attack at $\lambda = 6.13$ (a), the design configuration $\lambda = 4.08$ (b) and the high angle of attack $\lambda = 3:5$ (c). For all angles of attack, the pressure side flow is mainly of two dimensional charac-

ters, apart from the tip near region. The suction side flow at low angle of attack in sub-figure (a) shows reversal boundary layer flow at the trailing edge apart from the root near section and a small part next to the tip. The tangential flow direction can be distinguished in the plots with additional effect of centrifugal acceleration on the boundary layer flow.
The dark lines, which refer to an accumulated flow, are a clear indication of a reversed boundary layer flow and thus separation. At the design angle of attack, the separated strip at the trailing edge is wider than at low angle of attack. The root near section is characterized by radial velocity components, which originate from the rotational effects, namely Coriolis and centrifugal acceleration. At high angle of attack, the trailing edge separation is largely increased. In the span-wise middle section of the blade, the flow is separated over approximately half the chord length. On the suction side separation also occurs near the leading edge. The flow is separated and re-attaches, thus forming a separation bubble, due to Miley et al. 1982.

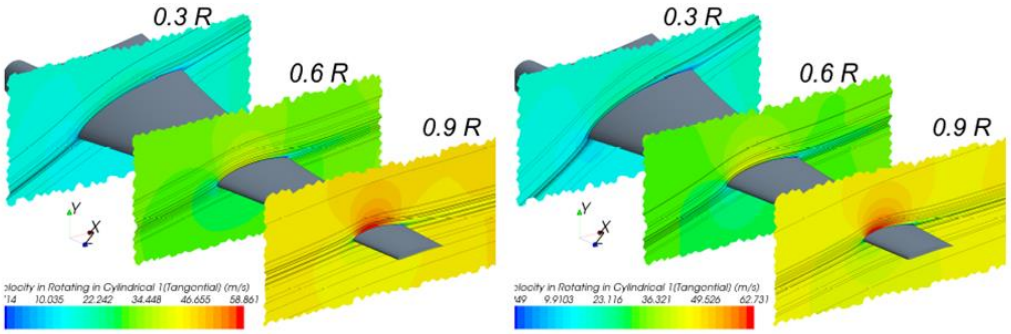

(a) Low α; $v_1 = 8\frac{m}{s}$, $\omega = 196$, $\lambda = 6.13$

(b) Low α; $v_1 = 10\frac{m}{s}$, $\omega = 196$, $\lambda = 4.90$

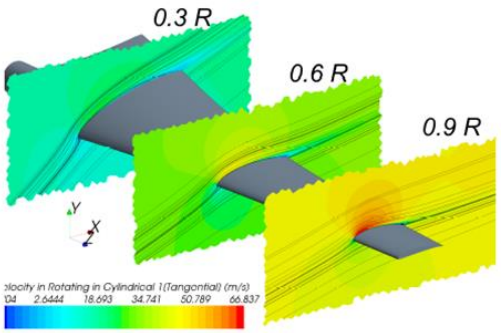

(c) Design α; $v_1 = 12\frac{m}{s}$, $\omega = 196$, $\lambda = 4.08$

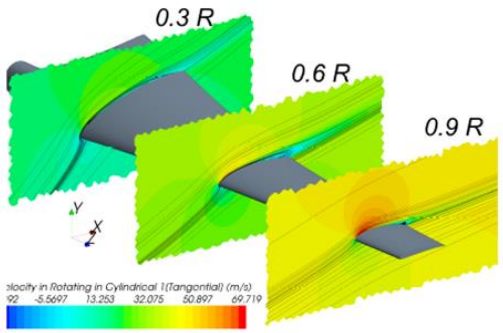

(d) High α; $v_1 = 14\frac{m}{s}$, $\omega = 196$, $\lambda = 3.5$

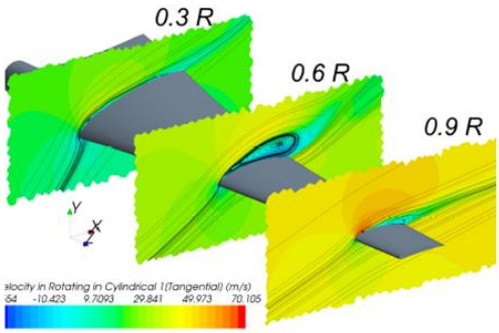

(e) High α; $v_1 = 16\frac{m}{s}$, $\omega = 196$, $\lambda = 3.06$

Figure 4: Tangential velocity on 2-D blade sections with velocity streamlines at low, design and high angle of attack

For the tip near flow the separation bubble does not form. The non-existing trailing edge separation at the root near section agrees with the theory of suppressed boundary layer separation near the root, through Coriolis and centrifugal forces, as outlined by Shen 1999. For the design and high angle of attack configurations, the flow is not solely in chord-wise direction but of three-dimensional character, for large parts of the blade.

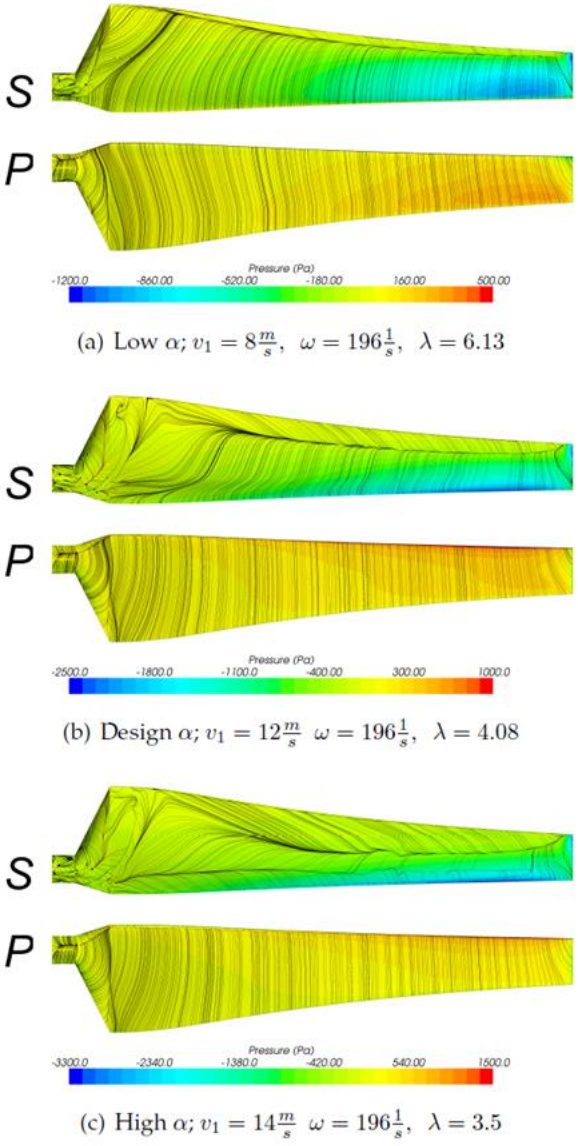

Figure 5: Pressure distribution and blade streamlines at different angles of attack

Conclusion

The aim of the present study is to get a better understanding of the aerodynamics of an optimized wind turbine rotor model. Further, the capability of the applied CFD methods was investigated. The simulations were performed as steady state with the RANS k-ω SST turbulence model. The main conclusions drawn from the simulations are:

- With the described simulations approach, the power coefficient is in agreement with the experimental data for the angles of attack below stall.
- The simulations give a clear indication for the beginning of stall.
- The three-dimensional character of the flow on the blade, especially near the root and tip, is shown in the simulations.

The study showed that the trailing edge separation near the root is suppressed by rotational effects, e. g. coriolis and centrifugal forces.

Acknowledgment

We would like to extend our thanks to the German Academic Exchange Service (DAAD) for providing their support to Mr. Al-Abadi.

References

SUMNER, J. ; WATTERS, C.S. ; MASSON, C.: CFD in Wind Energy: The Virtual, MultiscaleWind Tunnel. Energies (2010)

CARCANGIU, C.E. ; SOERENSEN, J.N. ; CAMBULI, F. ; MANDAS, N.: CFD-RANS analysis of the rotational effects on the boundary layer of wind turbine blades. Journal of Physics (2007)

MAHU, R. ; POPESCU, F. ; FRUNZULICA, F. ; DUMITRACHE, Al.: 3D CFD Modeling and Simulation of NREL Phase VI ROTOR. In: Proceedings to American Institute of Physics Conference (2011)

ANJURI, E.R.: Comparison of Experimental results with CFD for NREL Phase VI Rotor with Tip Plate. In: INTERNATIONAL JOURNAL of RENEWABLE ENERGY RESEARCH (2012)
KIRRKAMM, N. ; STOEVESANDT, B. ; GOLLNICK, B. ; PEINKE, J.: SIMULATION OF A MULTI MEGAWATT WIND TURBINE WITH OPENSOUCE CODE OPENFOAM. Poster at European Wind Energy Conference & Exhibition 2010 (2010)
CARCANGIU, C.E.: CFD-RANS Study of Horizontal Axis Wind Turbines, Universitae degli Studi di Cagliari, Diss., 2008
VERMEER, L.J. ; SOERENSEN, J.N. ; CRESPO, A.: Wind turbine wake aerodynamics. Progress in Aerospace Sciences (2003)
WUSSOW, S. ; SITZKI, L. ; HAHM, T.: 3D-simulation of the turbulent wake behind a wind turbine. Journal of Physics (2007)
AL-ABADI, A. ; ERTUNC, O. ; WEBER, H. ; DELGADO, A.: A Torque Matched Aerodynamic Performance Analysis Method for the Horizontal Axis Wind Turbines. WIND ENERGY (2013)
HIRSCH, C.: Numerical Computation of Internal and External Flows. Butterworth-Heinemann, (2008)
CD-ADAPCO: Star CCM+ 8.02 User Guide. (2013)
MENTER, F.R. ; KUNTZ, M. ; LANGTRY, R.: Ten Years of Industrial Experience with the SST Turbulence Model. Turbulence, Heat and Mass Transfer (2003)
MILEY, S.J.: A CATALOGUE OF LOW REYNOLDS NUMBER AIRFOIL DATA FOR WIND TURBINE APPLICATIONS / Department of Aerospace Engineering Texas A&M University. (1982)
SHEN, W.Z. ; SOERENSEN, J.N.: Quasi-3D Navier-Stokes Model for a Rotating Airfoil. Journal of Computational Physics (1999)